Empowering Clean Water whilst Safeguarding Water Distribution Pipeline Integrity: Towards Manganese- and Iron-Free Lime Hydrate for Water Treatment

Dávid Kocsis,[*1,2,3] Rhys A. Ward,[2,3] Christopher R. Meyer,[*1]
Michael Thompson,[4] Timothy J. Prior,[4] Stephen M. Kelly,[3,4]
Nathan S. Lawrence,[2,3] Jay D. Wadhawan[*2,3]

[1]*Singleton Birch, Ltd., Melton Ross Quarries,*
Barnetby DN38 6AE, North Lincolnshire, United Kingdom.

[2]*Department of Chemical Engineering, The University of Hull,*
Cottingham Road, Kingston-upon-Hull HU6 7RX, United Kingdom.

[3]*Aura Innovation Centre, Bridgehead Business Park,*
Meadow Road, Hessle HU13 0GD, United Kingdom.

[4]*Department of Chemistry, The University of Hull,*
Cottingham Road, Kingston-upon-Hull HU6 7RX, United Kingdom.

[*]Corresponding authors:
E.mail: dkocsis@singletonbirch.co.uk (DK); cmeyer@singletonbirch.co.uk (CRM); j.wadhawan@hull.ac.uk (JDW)

Electronic Supplementary Information (ESI)

ESI1: Chalk and Limestone

Limestones are rocks containing essentially calcium carbonate.[S1] These can be formed through precipitation from water, usually in widespread but shallow seas (non-clastic, chemical or inorganic limestone), through the secretions or capture by aquatic organisms such as coral or microorganisms (biogenic limestone),[S2] or through the shells of dead sea creatures such as coccolithophores or foraminifera (bioclastic limestone – the grains and clasts are fossils which do not interlock, but rather are agglomerated and cemented in an ooze).[S3] Limestones often contain impurities such as clay and sands. In the United Kingdom, there are four common types of limestone: chalk, Carboniferous Limestone, oolitic limestone and magnesian limestone (dolomite, $CaCO_3.MgCO_3$).[S4] The members of the British Lime Association – the national trade organisation for industrial lime producers, use limestones quarried from either Carboniferous Limestone (Lhoist UK and Tarmac Buxton Lime) in the Peak District, or Cretaceous Chalk (Singleton Birch, Ltd.) in Humberside. We consider both limestones in turn.

Cretaceous Chalk is a friable limestone.[S5] This rock, extracted at the Melton Ross Quarries by Singleton Birch, Ltd. (with an output of over 1.5 MTe/yr),[S6] is of the Welton Formation.[S7] The Chalk, formed through the deposition of the planktonic algæ (such as *Haptophyta*),[S8] is micritic (<1% allochemical rock), and is classified as being of the Northern Province.[S9] This rock is significantly stronger, more dense and contains less moisture (moisture content is 8-10% for the Welton Formation)[S7] than that of the Southern Province,[S9,S10-S12] owing to the twin occurrence of pressure solution effects (cementing due to dissolution and re-precipitation reactions),[S13] and folding (pressure release) during the Alpine uplift.[S10,S14] Northern Province Chalk, which has greater faunal affinities with those of Germany, Poland and Russia, compared with the Chalk of the Anglo-Paris Basin,[S10,S15] was deposited in a deeper-water environment than for the Southern Province Chalk[S10,S16] – the nodular chalks and flint horizons are only weakly developed, and glauconitised and phosphatised hard-grounds are much less well-developed in Northern Province Chalk.[S16] This enables Northern Province Chalk to be used as a building stone, in for, example, Louth Park Abbey almost 900 years ago.[S17] The Chalk is characterised by calcitic particles (coccoliths in the size range of 0.5 – 4 μm within a matrix of larger, polygonal calcite crystals),[S12] with high porosity (*ca.* 22% for the Welton Formation),[S18] and, owing to it being more brittle than the Southern Province Chalk, is of high permeability (~0.01 – 10 m/day), through clean fractures.[S18]

The Chalk at Melton Ross Quarries has been reported as being extremely pure, containing 99% $CaCO_3$,[S5,S7] with flints (chert) that are, for the most part of the succession, rare.[S7] Detailed stratigraphy have been reported.[S7,S10] Certain flint bands are prominent, such as the semi-tabular, pink, Ferruginious Flint, which contains pyrite-coated fractures that have been oxidised to limonite or hæmatite.[S7] A variety of marl bands (argillaceous rocks) are dispersed throughout the formation.[S7,S10] Although the Welton Chalk is softer than the overlying

Burnham Chalk, it is still indurated, with both a lateral and vertical variation in this hardness.[S10] Accordingly, Chalk is currently blasted from the outcrop from *ca.* 2 m above the Ferruginious Flint to between the Barton Marls 2 and 1, having previously been taken from deeper lithographies (from about 3 m above the Croxton Marl to about 2 m above the organic matter derived Black Band). As demonstrated in Electronic Supplementary Information ESI5, X-ray powder diffraction of a sample from the current quarry face confirms that the only crystalline phase present is calcite. Digestive analysis through ICP-OES (see Electronic Supplementary Information ESI4) revealed that the manganese level in chalk derived from the current quarry face is 30 mg/kg less than that from the deeper Welton Chalk lithographies previously quarried.

The Bee Low Limestone in Derbyshire is quarried by two UK lime manufacturers: Lhoist and Tarmac. This Carboniferous formation forms around 90% of the limestone outcrop in this area, and is of considerable economic importance.[S19,S20] The pale grey, limestone beds were deposited in an open-marine shelf environment, and are chert-free: they are typically lithographically uniform.[S19,S20] However, several clay bands (red-brown to green-grey), typically 0.5 m thick, are dispersed within the formation, thought to originate from the wide-spread, but intermittent falling of volcanic ash – volcanism was most active in the later part of the Dinantian.[S20] Nevertheless, the limestone is considered to be very high purity (CaO content is between 52.40 – 56.18 wt.%, with a mean of 55.41 ± 0.83 wt.%), with small impurities due to iron (Fe_2O_3 is reported to range between 70 – 31100 ppm, with a mean of 713 ± 2973 ppm) and manganese (MnO ranges between 40 – 700 ppm, with a mean of 119 ± 93 ppm).[S19,S20]

ESI2: Redox Boundaries in Groundwater Geochemistry

The redox potential (E_h, open-circuit potential *vs.* the Standard Hydrogen Electrode) of groundwater is an important parameter that marks its quality (chemical composition).[S21] For iron and manganese, this parameter is crucial as oxidised and reduced states have different (pH-dependent) aqueous solubilities. As an optimised parameter, however, E_h, which is measured as the potential of a platinum electrode with respect to a reference, is plagued by instabilities and experimental difficulties, since (1) the platinum surface can be fouled by both oxygen (forming platinum oxides) and hydroden sulfide (forming platinum sulfides), leading to inaccurate measurements under both oxic and anoxic conditions; (2) reactions can occur at the liquid junction of the reference electrode (including precipitation of heavy metal sulfides), causing measurement drift; and (3) the occurrence of mixed potentials during operations can give rise to poor reproducibility in measurements. Indeed, Whitfield[S22] has suggested that in the oxygenated environment of an unconfined aquifer, platinum electrodes behave as platinum oxide electrodes and respond to pH; in a confined aquifer environment, where H_2S is present, the slow formation of platinum sulfides pushes the value of E_h to more negative potentials. Nevertheless, E_h continues to be used as a convenient operational parameter to monitor changes in the redox system in flowing groundwater, as it is considered to provide an indication of the redox states of the water.[S23]

Manganese and iron ions are both redox active in bicarbonate-rich water at pH between[S24] 6.75 and 7.75. Under these conditions, divalent manganese (Mn^{2+}) and iron (Fe^{2+}) are soluble in water, but tetravalent manganese (MnO_2) and trivalent iron (FeOOH and $Fe(OH)_3$) are not. In the (Northern Province) Chalk aquifer of the East Riding of Yorkshire, for example, there is a small difference of *ca.* 300 mV in groundwater E_h on either side the former cliff-line buried in the Eemian (Ipswichian interglacial).[S25] This difference in redox potential (redox boundary) coincides with a change in dissolved oxygen (from >10 ppm to <4 ppm), and enables the hydrogeochemical mapping of the unconfined, semi-confined and confined aquifers.[S16,S25] Indeed, in the confined aquifer, Mn^{2+} and Fe^{2+} have been quantified at levels of as much as 100 and 1000 ppb, respectively, whilst in the unconfined and semi-confined aquifers, Mn^{2+} and Fe^{2+} have been measured to have levels below 20 and 50 ppb, respectively.[S16,S25]

A similar picture has been found in the (Southern Province) Chalk aquifer of the Anglo-Paris Basin:[S26] E_h values in the range 330-420 mV are associated with the unconfined aquifer, where dissolved oxygen levels are typically between 8-10 mg/L; these drop sharply to <160 mV with the complete disappearance of oxygen in the confined aquifer, which marks the redox boundary.[S26] It follows that such redox boundaries not only mark the changes in hydrogeochemistry, but also in the *chemistry of the trace redox elements in the aquifer rocks*.

ESI3: The Lime Cycle

The lime cycle refers to the process of mining calcium carbonate ($CaCO_3$), calcining this at temperatures up to 1100 °C to form quicklime (CaO), followed by hydration with water to yield slaked lime ($Ca(OH)_2$), which can be re-carbonated to $CaCO_3$ using carbon dioxide.[S27] As indicated in the Abstract of the main paper, the lime cycle is also used for dolomites.

At the Melton Ross Quarries, Singelton Birch, Ltd. manufacture slaked lime from quarried rock through the following typical manufacturing operations.

1. Limestone is blasted from the quarry face, to yield blocks typically in excess of 2 m. Unlike other limestones, the rock cannot be washed and cleaned with water, since the chalk is too friable.
2. The blocks are hauled into the primary crusher, which produces smaller stones (<200 mm in size) and fines. These are conveyed to the quarry fines plant, where very fine dust (< 5mm) is removed and supplied for use, whilst the remaining rocks are further conveyed to the stone blending plant, where they are separated by size into large (*ca.* 180 – 80 mm), medium (*ca.* 80 – 50 mm) and small (down to *ca.* 2 in). Small and medium stones are sorted optically, whilst the larger stones pass through X-ray sorting. These then pass through to the 180 Te storage hoppers, before waiting to enter the kiln in turn.
3. The sorted carbonate stones are fed, batch-wise, into the tops of highly efficient, gas-fired, vertical, Maerz PFR kilns, where they are calcined to afford calcium oxide. The top part of the kiln acts as a pre-heating zone, and is above the burning zone where the gas lances are located. As material falls below the gas lances, cold air is blown to cool the lime product. The kilns are fitted with a venturi scrubber, so as to remove any reactive lime particles from the flue gases, whilst at the same time abating both SO_2 (from the natural gas used) and CO_2 (from both gas combustion and carbonate decomposition) from the exhaust.
4. The produced lime (Burnt Lime 40) passes first to storage, and then is crushed and screened using a vibrating plate.
5. The majority of the screened lime is progressed to the hydrators, where reaction with a water spray takes place, to furnish the slaked lime product.
6. The oversize lime from the screen, if the quality is sufficiently high, is sent to the microlime plant, where the lime is further crushed to yield micron-sized lime (microlime 90), or processed through air classification to yield two lime products: one with size ≤ 45 μm and the rest (microlime 10-90).
7. Products are assessed for quality compliance, for example through analysis of the silica content, loss-on-ignition, *etc.*, and packed for storage, shipping and onward operations.

ESI4: Experimental Methods

Chemical Reagents

All manufactured samples of $CaCO_3$, CaO and $Ca(OH)_2$ were used, as received, from Singleton Birch, Ltd. This included a sample of lime hydrate derived from Carboniferous Limestone. The chalk, screenings and chalk-derived lime hydrate used were processed at the Melton Ross Quarries, from Cretaceous Chalk derived from both the middle stratitographic section (between the Melton Ross Marl and the Barton Marl 1) and the bottom bed (between the Grasby Marl, to just below the Chalk Hill Marl, but above the organic Black Band) of the Melton Ross Quarries. All other chemical reagents used were supplied by Fisher Scientific (aklaine sodium hypochlorite solution, laboratory grade), or Sigma-Adrich, with magnetite and maghæmite generously supplied by ParagonID, Ltd. Doubly deionised and filtered water, with a resistivity greater than 18 MΩ cm was taken from an Elgastat system (Vivendi). Oxygen and nitrogen were supplied by Air Products. Ozone was generated from a pure oxygen supply using an ozone generator (LAM2, Suez Water Technologies & Solutions).

Chemical Etching Methods

Unless otherwise specified, all experiments were undertaken under ambient temperature conditions (20 ± 2 ^{o}C). Chemical etching experiments were undertaken in triplicate, typically involved a 1 g of lime hydrate and 80 mL (100 g) of alkaline hypochlorite solution (8% or 14%), either in an open beaker under quiescent conditions (or stirred with a magnetic flea), or in a round-bottomed flask equipped with a Liebig condenser and refluxed at 90 ^{o}C for a fixed time period, in a fume cupboard. Ozone etching was undertaken under ambient temperature, using a similar volume of water as in the hypochlorite experiments, with continued bubbling of ozone in a stirred aqueous $Ca(OH)_2$ slurry for a specified length of time, in a fume cupboard. In both cases, pink supernatants were observed, which were removed through either vacuum filtration or centrifugation for spectrophotometric analysis. In the former case, the resulting filter cake was dried in an oven at 110 ^{o}C, and the upper part analysed *via* inductively coupled plasma-optical emission spectrometry (ICP-OES). For vacuum filtration, ceramic filters were preferred, since when paper-based filters were used, the filtrate changed colour[S28] from pink to blue and green, and then to yield a colourless solution! This could be due to the reduction of pink permanganate (MnO_4^-) to unstable blue hypomanganate (MnO_4^{3-}),[S29] and then to green manganate (MnO_4^{2-}), and ultimately yielding solid brown manganese dioxide (MnO_2), with the red ferrate ion (FeO_4^{2-}) being reduced to yellow ferric hydroxide ($Fe(OH)_3$), presumably by sulfite-derivatised celluloid fibres in the paper filter, formed during the paper pulping process.[S30] In the case of experimental cascade etches, the dried filter cake was used as the feed for each subsequent etch, with each feed appearing increasingly more "white".

For the case of experiments using calcite with gœthite (ironstone), the raw ironstone sample, generously supplied by Johnston Quarry Group, was broken up, and ground using an agate pestle and mortar. 1.0 g of this sample was refluxed with 80 mL of alkaline hypochlorite (14%) at 90 ^{o}C for 1 hr. The absence of a pink or red coloration was noted.

ICP-OES Analysis

Chalk, lime and lime hydrate contain silicate-based impurities. Accordingly, solid samples were first digested in HF: solid samples were weighed to four decimal place and transferred into PTFE digestion vessels. Sample size ranged typically from 0.1 - 0.5 g. A solution of 3 mL of concentrated nitric acid, 1 mL of concentrated hydrochloric acid (*i.e.* aqua regia) and 1 mL of 40% hydrofluoric acid were also added to each digestion vessel, to dissolve any silica present in the solid sample. All acids used were Romil super-purity spectroscopic grade. The digestion vessels were then closed and inserted into a carousel, which was then placed in a CEM Mars 5 microwave-assisted digester. Following a pre-set programme the vessel temperature was heated to 200 °C over a 15 min period, then was held constant at this temperature for a further 20 min. The temperature of the solution and pressures within digestion vessel were constantly measured in real time within the No 1 or control vessel. Pressures of 200 – 250 psi are typical at the higher temperatures. After cooling, each vessel was opened and 4mL of 4% spectroscopic grade boric acid was injected. The vessels were then placed back into the microwave and heated again to 170 °C in 15 min, and held at this temperature for 15 min. The addition of the boric acid “mops up” any remaining HF by forming BF_4^-. This second stage is required because samples containing free HF cannot be introduced into the ICP due to its internal glass components. After cooling again, the digests were then transferred to tared Sarstedt tubes. The digestion vessels were rinsed three times with ultra high quality (UHQ) water, the washings added to the tubes and the whole solution made up to 40 mL with UHQ water. The tubes were then weighed to four decimal places giving the weight of the digest, followed by their analysis for their iron and manganese contents by ICP-OES. The instrument used was a Perkin Elmer Optima 5300 DV, and each run was calibrated using Romil certified Standards.

Iron and manganese levels in the original solid samples were then calculated using the measured levels within the digest, the digest weight and the original sample weight.

Visible Spectroscopy

Visible spectroscopy of the pink supernatant was undertaken using a PerkinElmer Lambda-25-Scan-UV–Vis instrument, using a quartz cell of 1.0 cm path length.

X-Ray Powder Diffraction

Samples of chalk and lime hydrate derived from chalk were examined by X-ray powder diffraction performed on a PANAlytical Empyrean X-ray diffractometer (XRD) operating in

Bragg-Brentano geometry using copper $K\alpha_1$ radiation (λ = 1.54056 Å), and a PIXEL detector. Patterns were fitted and the phases present identified using the PDF2 database.[S31]

The pattern for the lime hydrate sample was fitted using Rietveld refinement[S32] to obtain a quantitative assessment of the amount of each crystalline phase present. The background was fitted using a nine-term shifted Chebyshev polynomial. Peaks were fitted using a pseudo-Voigt peak shape. For each phase, lattice parameters and profile parameters were refined. A single zero-point correction was refined. Preferred orientation in the portlandite phase was treated using standard methods.

ESI5: X-Ray Diffraction Studies of Chalk and Lime Hydrate

The X-ray powder diffraction pattern of chalk taken from the Melton Ross Quarries is shown in Figure S1. This confirms that the only crystalline phase present is calcite, which is highly crystalline.

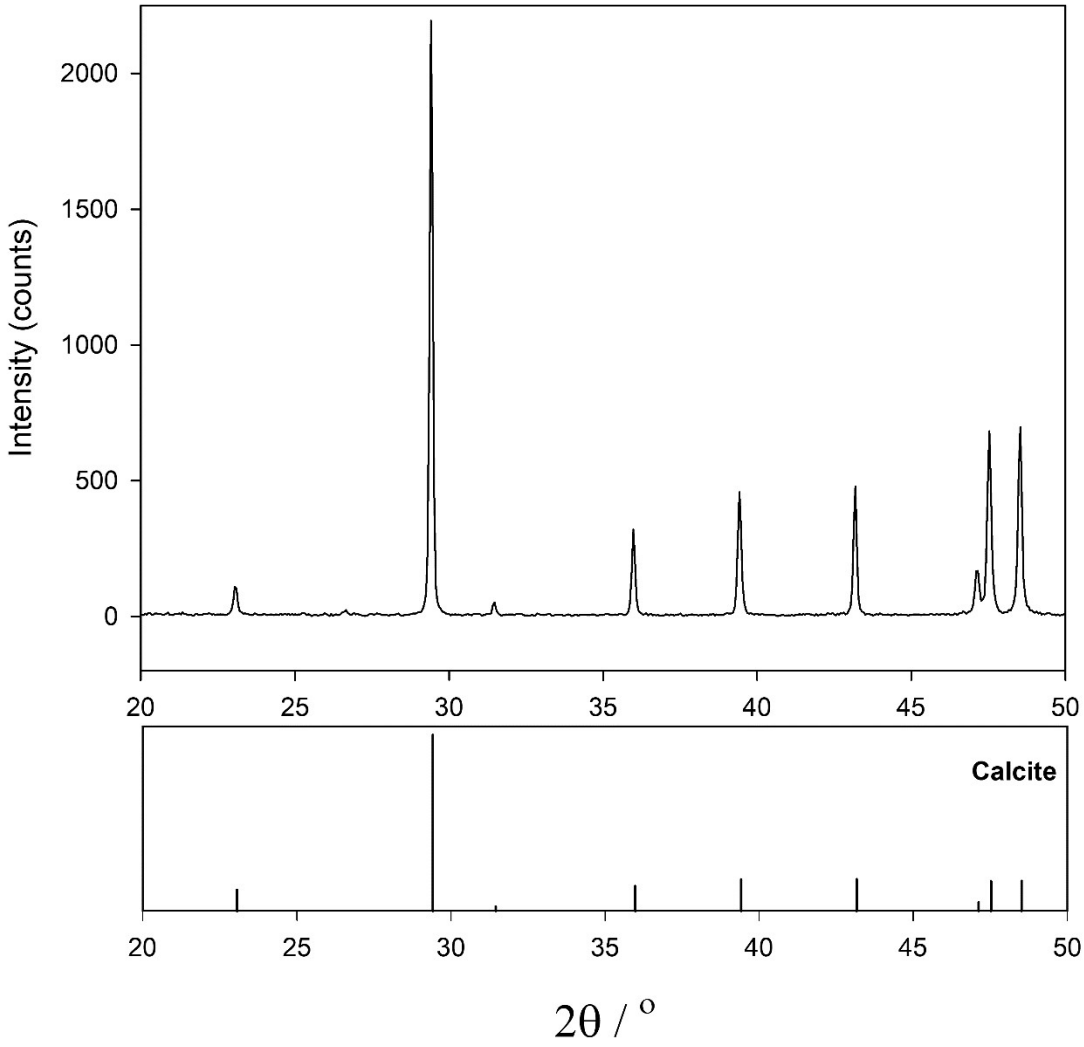

Figure S1: *X-Ray powder diffraction pattern of chalk. The lower panel shows the allowed peak positions for calcite and the relative peak intensities. The sample was of Welton formation Chalk derived from screenings obtained from the middle stratitographic section (between the Melton Ross Marl and the Barton Marl 1).*

The X-ray powder diffraction pattern of lime hydrate is shown in Figure S2. This sample contains two crystalline phases; the dominant phase is portlandite and there is a smaller amount of highly crystalline calcite. It was possible to fit the observed data using the Rietveld method and a good fit was obtained (R_p = 5.63 %). This revealed the sample contained portlandite and calcite in the ratio 97.2 : 2.8 ± 0.2 % by weight.

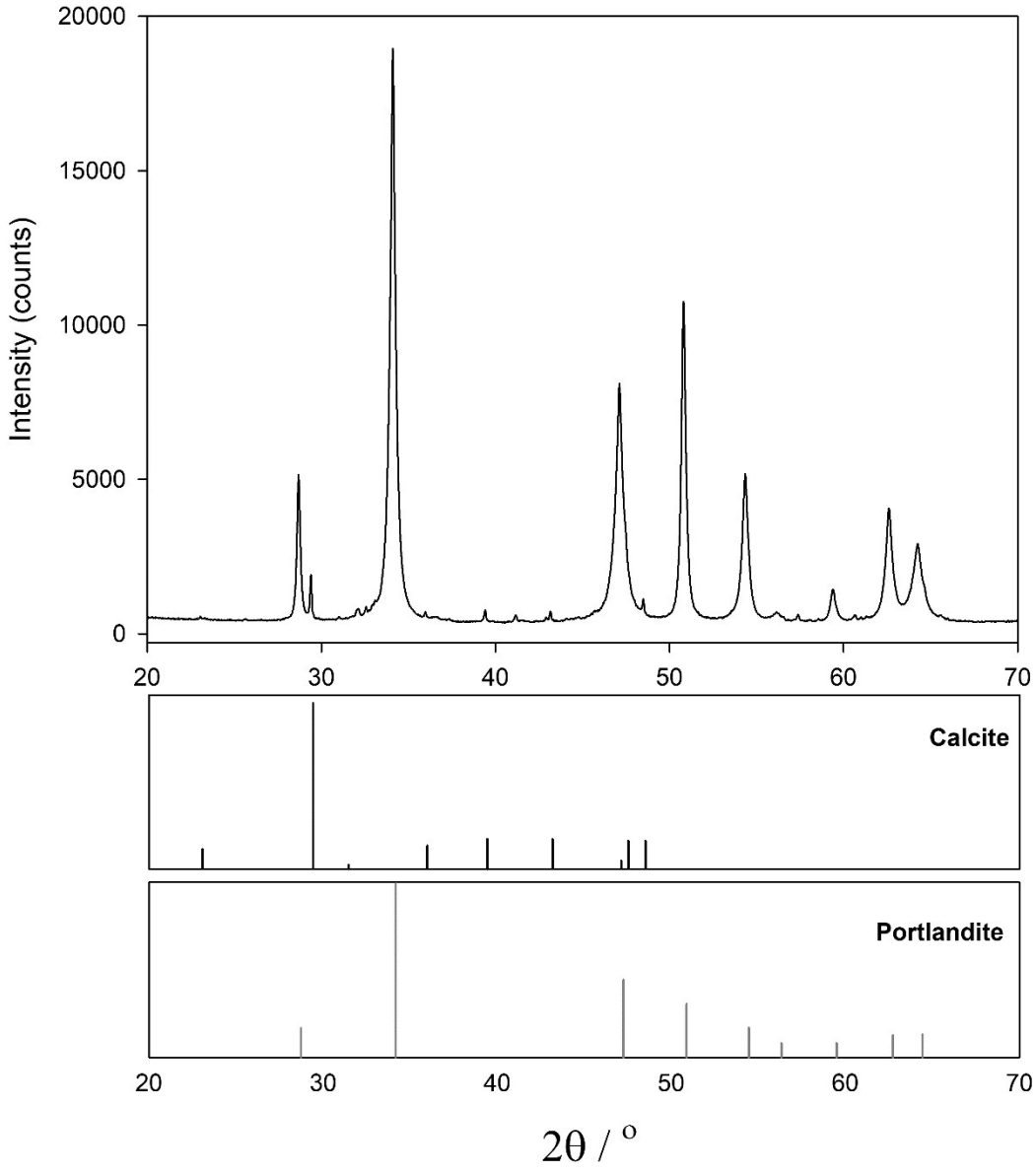

Figure S2: *X-Ray powder diffraction pattern of lime hydrate derived from Welton formation Chalk screenings obtained from the middle stratitographic section (between the Melton Ross Marl and the Barton Marl 1). The lower panels show the allowed positions and relative intensities of peaks for calcite and portlandite.*

Note that the ratio of portlandite to calcite was estimated through performing a routine two-phase Rietveld refinement, using GSAS implemented within EXP-GUI. The portlandite phase is well known to suffer from preferred orientation and this was treated using standard methods in GSAS employing spherical harmonics.[S33] The fit is less than ideal because of this effect but the fit indicators are reasonable: wR_p = 0.0895 and R_p = 0.0563. The fit to the observed data is shown in Figure S3.

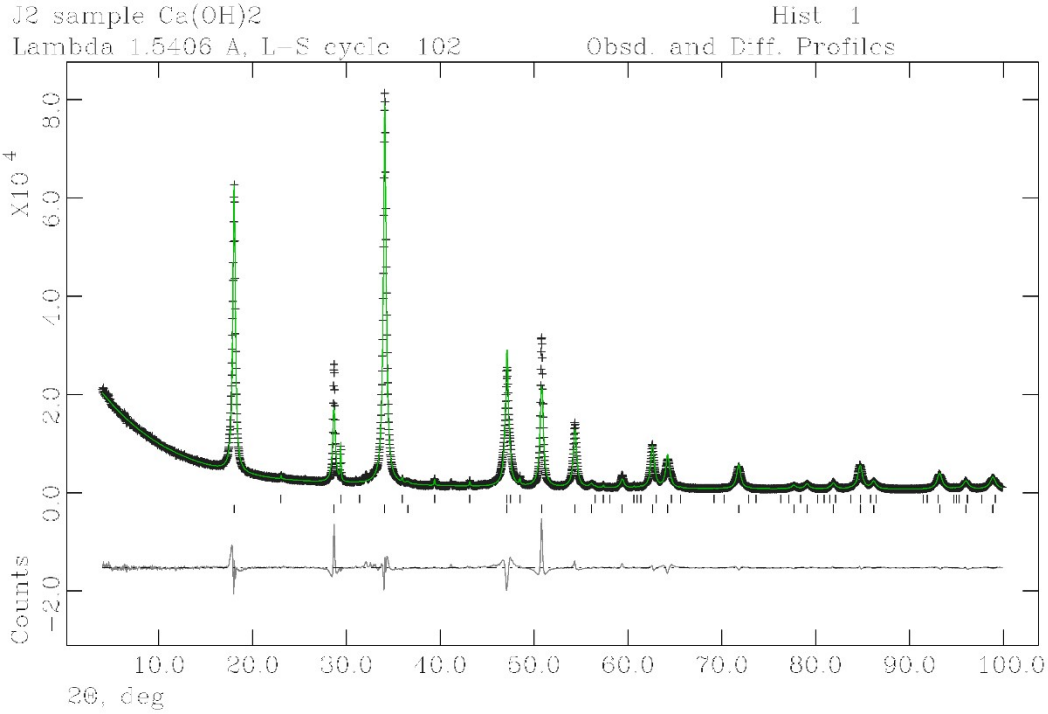

Figure S3: *X-Ray diffraction profiles for lime hydrate derived from Welton formation Chalk screenings obtained from the middle stratitographic section (between the Melton Ross Marl and the Barton Marl 1). Raw data are shown as black crosses; green line is the calculated pattern; the lower solid line is the difference plot. The upper tick marks represent allowed peak positions for calcite and the lower tick marks represent allowed peak positions for portlandite.*

ESI6: Spectroscopic Evidence of MnO_4^- and FeO_4^{2-}

Figure S4 illustrates the visible spectrum of the pink supernatant obtained on incubating lime hydrate with alkaline hypochlorite at under ambient conditions for 72 hr. The split-peak at *ca.* 520 nm fingerprints the permanganate (MnO_4^-) anion, with the two further peaks at *ca.* 495 nm, and 540 nm, which match-up with that expected from ferrate (FeO_4^{2-}).[S34]

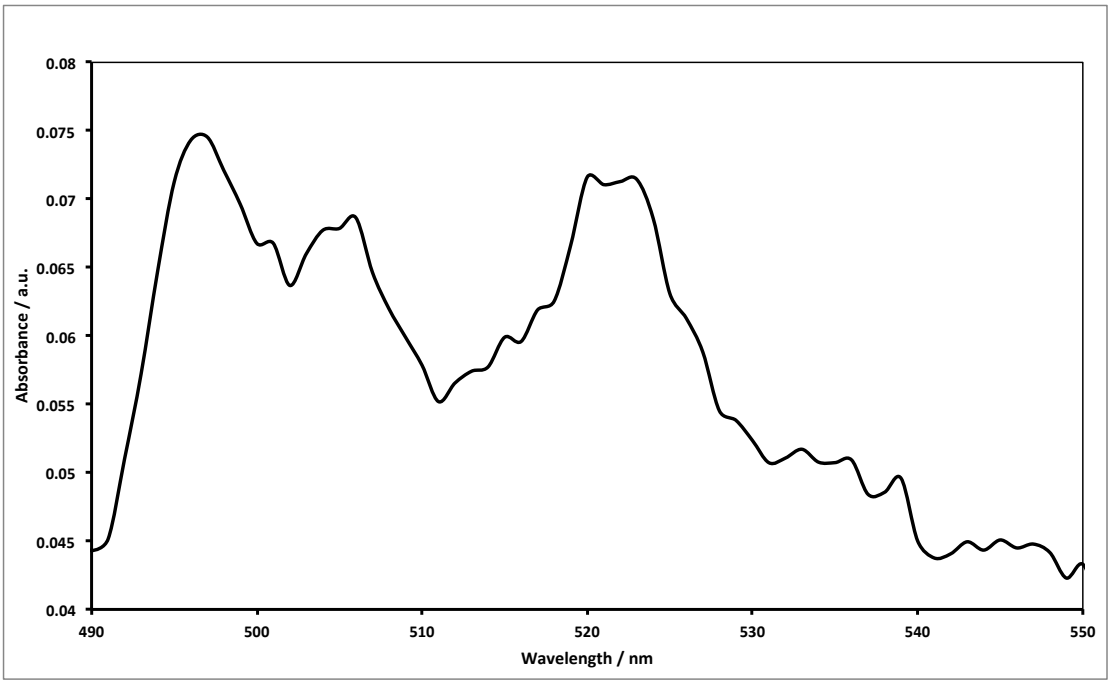

Figure S4: *Spectrophotometric fingerprinting of MnO_4^- and FeO_4^{2-} present in the supernatant following incubation of lime hydrate derived from Welton formation Chalk screenings obtained from the middle stratitographic section (between the Melton Ross Marl and the Barton Marl 1), with alkaline hypochlorite.*

ESI7: Experiments with an Ironstone

A sample of Great Tew Ironstone (Great Tew, Chipping Norton, Oxfordshire, UK) was generously provided by Johnston Quarry Group. The sample was crushed in an agate pestle and mortar, and analysed by X-ray diffraction, see Figure S5.

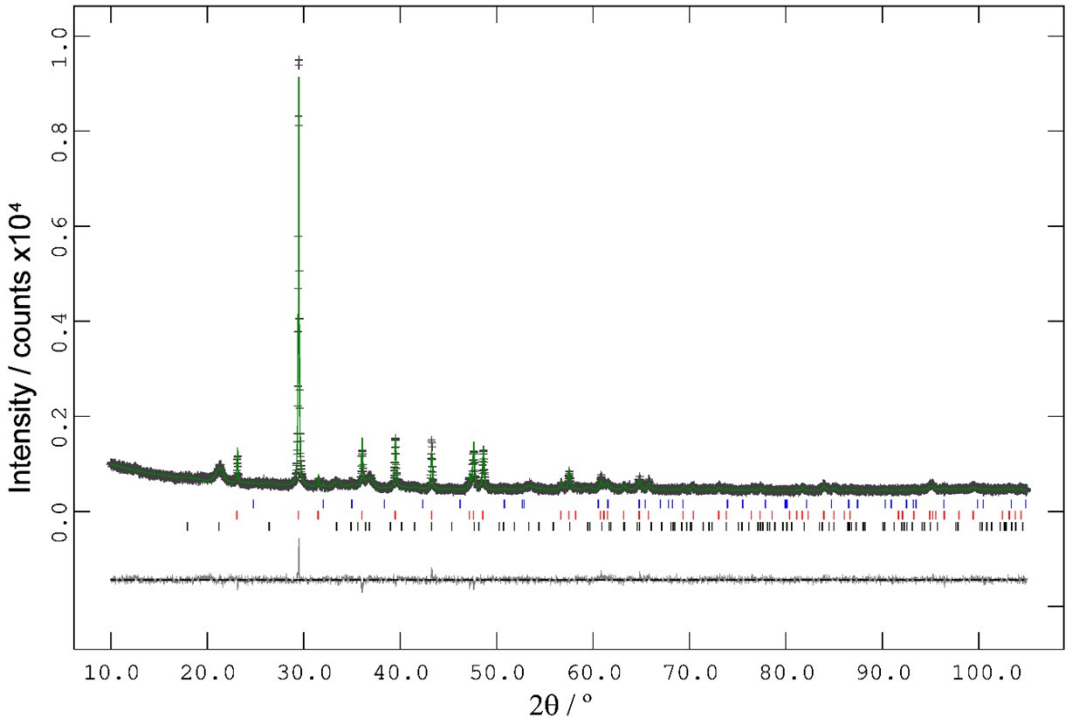

Figure S5: *X-Ray diffraction profiles for ironstone derived from Great Tew quarry. Raw data are shown as grey crosses; green line is the calculated pattern; the lower solid line is the difference plot. The upper tick marks represent allowed peak positions for siderite; middle tick marks show allowed peak positions for calcite; the lower tick marks represent allowed peak positions for gœthite.*

The X-ray powder diffraction pattern is dominated by peaks of calcite, with a smaller amount of gœthite and a trace amount of siderite. It was possible to undertake undertake quantitative analysis of the diffraction data using the Rietveld method and a good fit was obtained (R_p = 3.48 %). The composition of the sample by weight is calcite 82.4(3)%, goethite 17.2(3)%, and siderite (0.43(7)%).

The analysis is complicated by the fact that the powder diffraction pattern of siderite is dominated by a single peak vastly more intense than the others; here that peak is 100 times less intense than the strongest peak for calcite. Accordingly, a zoom-in on the low angle region helped identify the three phases (see Figure S6).

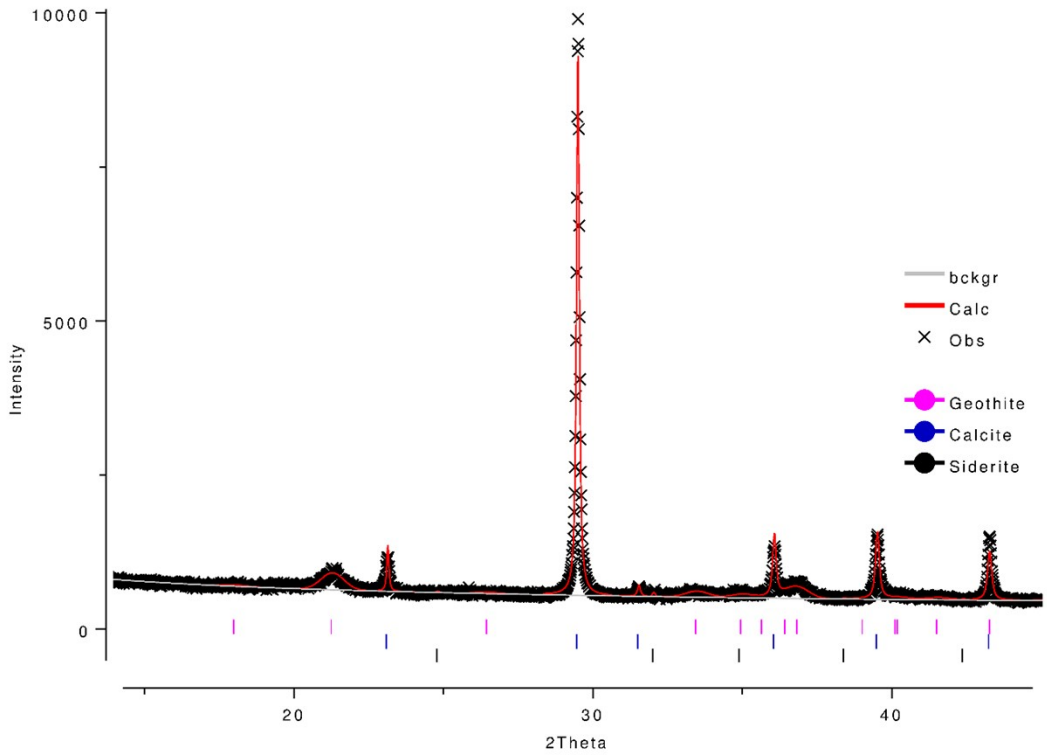

Figure S6: *X-Ray powder diffraction pattern of Great Tew Ironstone with raw data shown as black crosses in the range 15 < 2 θ/° < 45. Upper tick marks show allowed peak positions of gœthite; middle ticks show allowed peak positions of calcite; lower tick marks show peak positions for siderite.*

Refined unit cell parameters for the three phases are given below.

	a / Å	**b / Å**	**c / Å**	**α / °**	**β / °**	**γ / °**	**Volume / Å^3**	**Space group**
Gœthite	9.862(4)	3.0044(12)	4.6143(18)	90	90	90	136.72(7)	*Pnma*
Calcite	4.98156(15)	4.98156(15)	17.0285(6)	90	90	120	365.96(3)	*R* -3 *c*
Siderite	4.687(2)	4.687(2)	15.417(11)	90	90	90	293.34(19)	*R* -3 *c*

Quality of fit factors (31 variables):

wRp (fitted)	Rp (fitted)	wRp (no background)	Rp (no background)	χ^2
0.0451	0.0348	0.0686	0.0491	1.147

ESI8: Retrograde Solubility of $Ca(OH)_2$ with Temperature

We consider the solubility equilibrium for calcium hydroxide in water:

$$Ca(OH)_2(s) \rightleftarrows Ca^{2+}(aq) + 2OH^-(aq) \quad \text{(S1)}$$

for which the solubility product is[S35] $K_{sp} = a_{Ca^{2+}}\left(a_{OH^-}\right)^2 = 4.68 \times 10^{-6}$ at 25 °C (yielding a solution of pH 12.3). Assuming the standard enthalpy change for this dissolution equilibrium is independent of temperature (*viz.*, $\Delta H^0 = -12.60\ kJ/mol$, based on the value calculated using standard enthalpies of formation, and validated experimentally),[S36] the van't Hoff equation, $\ln\left\{\frac{(K_{sp})_{T=T_2}}{(K_{sp})_{T=T_1}}\right\} = \frac{\Delta H^0}{R}\left(\frac{T_2 - T_1}{T_1 T_2}\right)$, enables the estimation of the temperature dependence of the solubility product. We find that at 20 °C, K_{sp} = 5.10 x 10^{-6}, and at 90 °C, K_{sp} = 1.88 x 10^{-6}. Assuming activity coefficients are unity, this corresponds to lime hydrate solubilities of 0.80 g/L at 20 °C, which reduces to 0.58 g/L as the temperature increases to 90 °C. This is the retrograde solubility of lime hydrate with temperature – the solubility of $Ca(OH)_2$ decreases with temperature, in agreement with experimental observations.[S36,S37]

It follows that, at the ambient temperatures used in this work (20 °C), in 80 mL of pure water, 1.0 g of pure $Ca(OH)_2$ (mole fraction ratios 0.003 : 0.997) will lose only 6.4% of its mass through dissolution; this decreases to 4.6 wt.% at 90 °C. However, these values are decreased further by the common-ion effect in the alkaline hypochlorite solutions used (alkalinity ≤ 2% by mass, density ~1.25 g/mL), where the hydroxide ion concentration is estimated as 0.6 M (recognising that sodium hydroxide solutions are hygroscopic), corresponding to pH ~ 13.8. Under these conditions, at 20 °C, the solubility of $Ca(OH)_2$ reduces to 1.1 mg/L, so that only 0.01% (by mass of $Ca(OH)_2$ would dissolve under the typical experimental conditions used. The retrograde solubility of $Ca(OH)_2$ causes this dissolutive loss to reduce to 0.003 wt.% by mass at 90 °C. This loss is essentially negligible at the experimental scale considered in this work.

ESI9: Zeroth-Order Heterogeneous Kinetics for Impurity Dissolution

The observation of zeroth-order heterogeneous kinetics results from (1) a very slow rate constant for the oxidative etching process, and (2) the large concentrations of the hypochlorite (or ozone) oxidant, as demonstrated below.

We consider the case where the manganese surface impurity of an inert solid, spherical particles (monodisperse in size) dissolves when suspended and mixed uniformly in an aqueous solution containing an oxidant (of bulk concentration c_0). The surface reaction flux (j_{int}):

$$j_{\text{int}} = k_s c_{\text{int}} \tag{S2}$$

comprises the product of the interfacial concentration of the oxidant (c_{int}) and the interfacial rate constant (k_s, given in length per unit time). This interfacial rate constant is the product of the surface coverage of the manganese impurity (as amount per unit area, Γ_{Mn}) and a "true" heterogeneous rate constant, k_s^0: $k_s = k_s^0 \Gamma_{Mn}$. The mass transport flux (j_{sol}) of chemical oxidant to the surface is given by:

$$j_{sol} = k_L \left(c_0 - c_{\text{int}}\right) \tag{S3}$$

in which k_L is the mass transfer coefficient. The flux expressions in (S2) and (S3) are equal at the interface,[S38] yielding,

$$c_{\text{int}} = \frac{k_L}{k_s + k_L} c_0 \tag{S4}$$

Since the dissolutive rate of reaction ($\frac{d[Mn]}{dt}$) is given by $\frac{d[Mn]}{dt} = -j_{\text{int}} \frac{S}{V}$, where [Mn] is the concentration of the manganese impurity in the solid, S is the total interfacial area exposed for reaction and V is the total volume of the solid particles, we find,

$$-\frac{d[Mn]}{dt} = \frac{k_s k_L}{k_s + k_L} \frac{S}{V} c_0 = \frac{3}{r_0} \frac{k_s k_L}{k_s + k_L} c_0 = \frac{3}{\sqrt[3]{\frac{3m}{4\pi N \rho}}} \frac{k_s k_L}{k_s + k_L} c_0 \tag{S5}$$

where r_0 is the radius of the inert solid particles, ρ is the density of the inert solid, m is the mass of the inert solid and N is the number of solid particles present. Thus, from equation (S5), monodispersity in the solid causes limited, if any, variation in the dissolution rate with mass of solid present. Thus, in the limit when the mass transport is faster than the surface dissolution reaction, the dissolution rate is given by,

$$-\frac{d[Mn]}{dt} \approx \frac{3}{\sqrt[3]{\frac{3m}{4\pi N \rho}}} k_s c_0 \tag{S6}$$

Since the manganese impurity is present at a trace level compared with the oxidant, all of the variables on the right-hand side of equation (S6) are effectively constant, leading to the observation of zeroth-order heterogeneous reaction kinetics. Since equation (1) in the main paper is in terms of the number moles of the manganese impurity, *viz.*, $\frac{d\left(n_{Mn}\right)_{solid}}{dt} = -k_{het}$, it

follows that $k_{het} \approx 4\pi r_0^2 k_s c_0 = 4\pi \left(\frac{3m}{4\pi N \rho} \right)^{2/3} k_s c_0$ is effectively constant since k_s is tiny and m/N is fixed for monodisperse particle distributions. Note that these relationships assume that the particle size remains constant throughout the impurity removal process, since it is assumed that only the impurity dissolves. This distinguishes these expressions from those developed for the surface-controlled, complete dissolution of both liquid[S39] and solid[S40] microparticles discussed in the published literature.

ESI10: ESI References and Notes

S1. See, for example, (a) T. Crook, The origin of limestones, *Nature*, 1924, **114**, 733; (b) W. G. Moore, *A Dictionary of Geography*, 3rd edn., Penguin Books, Harmondsworth, Middlesex, 1963

S2. See, for example, M. Rogerson, H. M. Pedley, J. D. Wadhawan, R. Middleton, New insight into biological influence on the geochemistry of freshwater carbonate deposits, *Geochim. Cosmochim. Acta*, 2008, **72**, 4976.

S3. See, for example, D. L. Holmes, *Elements of Physical Geology*, Thomas Nelson and Sons, London, 1969.

S4. See, for example, M. J. Bradshaw, *A New Geology*, Hodder and Stoughton, London, 1973.

S5. J. M. Hancock, The petrology of the Chalk, *Proc. Geol. Ass.*, 1975, **86**, 499.

S6. D. J. Harrison, F. M. McEvoy, P. J. Henney, D. G. Cameron, E. J. Steadman, S. F. Hobbs, N. A. Spenser, D. J. Evans, G. K. Lott, E. M. Bartlett, M. H. Shaw, D. E. Highley, T. B. Colman, *Mineral Resource Information in Support of National, Regional and Local Planning – Humberside (comprising East Riding of Yorkshire, North Lincolnshire, North-East Lincolnshire and City of Kingston-upon-Hull*, British Geological Survey Commissioned Report CR/04/227N, British Geological Survey, Keyworth, 2005.

S7. (a) G. D. Gaunt, T. P. Fletcher, C. J. Wood, *Geology of the Country Around Kingston-upon-Hull and Brigg: Memoir for 1:50000 geological sheets 80 and 89 (England and Wales)*, British Geological Survey, Her Majesty's Stationary Office, London, 1992; (b) F. Whitham, The geology of the Melton Ross chalk quarries, *Humber Geologist*, No. 12, Hull Geological Society, Kingston-upon-Hull, 1999, available online: http://www.hullgeolsoc.co.uk/meltonrs.htm (accessed December 28, 2021).

S8. J. M. Hancock, M. Price, Real chalk balances the water supply, *J. Wine Res.*, 1990, **1**, 45.

S9. M. G. Sumbler, *The Statigraphy of the Chalk Group in Yorkshire and Lincolnshire*, British Geological Survey Technical Report, WA/99/02, British Geological Survey, Keyworth, 1999.

S10. R. N. Mortimore, *Logging the Chalk*, Whittles Publishing, Dunbeath, Caithness, 2014.

S11. C. J. Wood, E. G. Smith, Lithostratigraphical classification of the Chalk in North Yorkshire, Humberside and Lincolnshire, *Proc. Yorks. Geol. Soc.*, 1978, **42**, 263.

S12. J. I. Pitman, Groundwater geochemistry and mass transfer in the East Yorkshire Chalk, in J. C. Crips, F. G. Bell, M. G. Culshaw (eds.), *Groundwater in Engineering Geology*, Geological Society Engineering Geology Special Publication No. 3, Geological Society, London, 1986, p. 177.

S13. A. C. Fowler, X. Yang, Pressure solution and viscous compaction in sedimentary basins, *J. Geophys. Res.*, 1999, **104**, 12989.

S14. C. V. Jeans, D. Long, X.-F. Hu, R. N. Mortimore, Regional hardening of Upper Cretaceous Chalk in eastern England, UK: trace element and stable isotope patterns in the Upper Cenomanian and Turonian Chalk and their significance, *Acta Geol. Polon.*, 2014, **64**, 419.

S15. S. F. Mitchell, The Chalk group (Upper Cretaceous) of the Northern Province, eastern England – a review, *Proc. Yorks. Geol. Soc.*, 2019, **62**, 153.

S16. P. L. Smedley, I. Neumann, R. Farrell, *Baseline Report Series 10: The Chalk Aquifer of Yorkshire and North Humberside*, British Geological Survey Commissioned Report No. CR/04/128, British Geological Survey, Keyworth, 2004.

S17. P. Kent, *Eastern England: From the Tees to The Wash*, 2nd edn., British Regional Geography series for the Institute of Geological Sciences, Her Majesty's Stationary Office, London, 1980.

S18. I. N. Gale, H. K. Rutter, *The Chalk Aquifer of Yorkshire*, British Geological Survey Research Report RR/06/04, British Geological Survey, Keyworth, 2006.

S19. (a) Department of the Environment, *Appraisal of High-Purity Limestones in England and Wales: A Study of Resources, Needs, Uses and Demands: Summary Report*, Department of the Environment, London, 1990; (b) D. J. Harrison, J. M. Hudson, B. Cannell, *Appraisal of High-Purity Limestones in England and Wales: A Study of Resources, Needs, Uses and Demands: Part 1: Resources*, British Geological Survey Mineral Resources Series WF/90/10, British Geological Survey, Keyworth, 1991; (c) D. J. Harrison, High-purity limestones in England and Wales, *Quart. J. Eng. Geol.*, 1993, **26**, 293; (d) D. J. Harrison, D. Highley, A. Bloodworth, R. Bate, D. Cameron, P. Lusty, D. Rayner, *Limestone*, Mineral Planning Factsheet prepared for the Office of the Deputy Prime Minister, British Geological Survey, Keyworth, 2006, available to download from http://www.mineralsUK.com (accessed December 28, 2021); (e) C. Mitchell, High-purity limestone quest, *Industrial Minerals*, 2011, 48.

S20. (a) D. J. Harrison, *The Limestone and Dolomite Resources of the Country Around Buxton, Derbyshire: Description of 1:25000 sheet SK 07 and parts of SK 06 and 08*, Mineral Assessment Report 77 for the Institute of Geological Sciences, Her Majesty's Stationary Office, London, 1981; (b) D. J. Harrison, K. A. McL. Adlam, *Limestones of the Peak: A Guide to the Limestone and Dolomite Resources of the Peak District of Derbyshire and Staffordshire: Description of parts of 1:50000 geological sheets 99, 111, 112, 124 and 125*, Mineral Assessment Report 144 for the British Geological Survey, Her Majesty's Stationary Office, London, 1985.

S21. See, for example, D. K. Todd, L. W. Mays, *Groundwater Hydrology*, 3rd edn., Wiley, New Delhi, 2005.
S22. M. Whitfield, Thermodynamic limitations on the use of the platinum electrode in E_h measurements, *Limnol. Oceanogr.*, 1974, **19**, 857.
S23. P. Shand, W. M. Edmunds, A. R. Lawrence, P. L. Smedley, S. Burke, *The Natural (Baseline) Quality of Groundwater in England and Wales*, Environment Agency Technical Report NC/99/74/24, Groundwater Programme Research Report RR/07/06, British Geological Survey, Keyworth, 2007.
S24. D. R. Champ, J. Gulens, R. E. Jackson, Oxidation-reduction sequences in groundwater flow systems, *Can. J. Earth Sci.*, 1979, **16**, 12.
S25. P. L. Smedley, B. R. Gibbs, J. M. Trafford, *National Groundwater Survey: Chalk Aquifer Study – Hydrogeochemistry and Water Quality of the Chalk Aquifer of North Humberside and Yorkshire*, Hydrology Series Technical Report WD/96/80C, British Geological Survey, Keyworth, 1996.
S26. W. M. Edmunds, W. G. Darling, D. G. Kinniburgh, L. Dever, P. Vachier, *Chalk Groundwater in England and France: Hydrogeochemistry and Water Quality*, British Geological Survey Research Report SD/92/2, Keyworth, 1992.
S27. K. van Balen, Understanding the lime cycle and its influence on historical construction practice, in S. Huerta, I. Juan de Herrera, A. E. Benvenuto, F. Dragados (eds.), *Proceedings of the First International Congress on Construction History*, Madrid, January 20-24, 2003.
S28. See, for example, S. G. Simpson, The effect of the presence of filter paper on permanganate-oxalate titrations, *J. Ind. Eng. Chem.*, 1921, **13**, 1152
S29. The blue pentavalent manganese ion hypomanganate has only ever been observed in strongly alkaline solutions, where it is known to be unstable. See, for example, the electrochemical generation of hypomanganate: (a) H. H. Miller, L. B. Rogers, Pentavalent manganese, *Science*, 1949, **109**, 61; or its generation through reaction with sulfite to yield MnO_2: (b) L. I. Simandi, M. Jaky, Z. A. Schelly, Short-lived manganate(VI) and manganate(V) intermediates in the permanganate oxidation of sulfite ion, *J. Am. Chem. Soc.*, 1984, **106**, 6866. The characteristic blue colour is discussed in (c): L. E. Orgel, The visible spectrum of the hypomanganate ion, *Molec. Phys.* 1964, **7**, 397.
S30. See, for example, G. T. Austin, Shreve's Chemical Process Industries, fifth ed., McGraw-Hill, New York, USA, 1984.
S31. S. Gates-Rector, T. Blanton, The powder diffraction file: a quality materials characterization database. *Powder Diffraction*, 2019, **34**, 352.
S32. L. B. McCusker, R. B. von Dreele, D. E. Cox, D. Louer, P. Scardi, Rietveld refinement guidelines, *J. Appl. Cryst.* 1999, **32**, 36.
S33. M. A. G. Aranda, A. G. De la Torre, L. León-Reina, Powder diffraction characterisation of cements, in C. J. Gilmore, J. A. Kaduk, H. Schenk (eds.), *International Tables for Crystallography*, volume H, chapter 7.12, Wiley, Chichester, 2019, p. 856
S34. (a) S. Licht, V. Naschitz, L. Halperin, L. Lin, J. Chen, S. Ghosh, B. Liu, Analysis of ferrate(VI) compounds and super-iron Fe(VI) battery cathodes: FTIR, ICP, titimetric, XRD, UV/VIS, and electrochemical characterisation, *J. Power Sources*, 2001, **101**, 167; (b) Y. L. Wang, S. H. Ye, J. K. Bo, Y. Y. Wang, F. Wu, Electrochemical reduction mechanism of Fe(VI) at a porus Pt black electrode, *J. Electrochem. Soc.*, 2009, **156**, A572; (c) S. Barışçı, F. Ulu, H. Särkkä, A. Dimoglo, M. Sillanpää, Electrosynthesis of ferrate(VI) ion using high purity iron electrodes: optimisation of influencing parameters on the process and investigating its stability, *Int. J. Electrochem. Sci.*, 2014, **9**, 3099; (d) Y.-L. Wei, Y.-S. Wang, C.-H. Liu, Preparation of potassium ferrate from spent steel pickling liquid, *Metals*, 2015, **5**, 1770; (e) J.-Q. Jiang, C. Stanford, M. Petri, Practical application of ferrate(VI) for water and wastewater treatment – site study approach, *Water-Energy Nexus*, 2018, **1**, 42; (f) B. Shao, H. Dong, X. Guan, Role of ferrate(IV) and ferrate(V) in activating ferrate(VI) by calcium sulphite for enhanced oxidation of organic contaminants, *Environ. Sci. Technol.*, 2019, **53**, 894; (g) P. C. W. Cheung, D. R. Williams, J. Barrett, J. Barker, D. W. Kirk, On the origins of some spectroscopic properties of "purple iron" (the tetroxoferrate(VI) ion and its Pourbaix safe-space, *Molecules*, 2021, **26**, 5266.
S35. D. R. Lide (ed.), *CRC Handbook of Chemistry and Physics*, 76th edn., CRC Press, Boca Raton, Fl., 1995.
S36. See, for example, (a) H. P. Hopkins, Jr., C. A. Wulff, The solution thermochemistry of polyvalent electrolytes: I: calcium hydroxide, *J. Phys. Chem.*, 1965, **69**, 6; (b) W. B. Euler, L. J. Kirschenbaum, B. Ruekberg, Determination of K_{sp}, ΔG^0, ΔH^0 and ΔS^0, *J. Chem. Educ.*, 2000, **77**, 1039.
S37. (a) J. Wang, T. C. Keener, G. Li, S.-J. Khang, The dissolution rate of $Ca(OH)_2$ in aqueous solutions, *Chem. Eng. Commun.*, 1998, **169**, 167; (b) S. Kilic, G. Toprak, E. Ozdemir, Stability of $CaCO_3$ in $Ca(OH)_2$ solution, *Int. J. Mineral Process.*, 2016, **147**, 1.
S38. (a) J. F. Zimmerman, Diffusion and activation control in heterogeneous reactions, *J. Phys. Chem.*, 1949, **53**, 562; (b) L.L. Bircumshaw, A. C. Riddiford, Transport control in heterogeneous reactions, *Q. Rev. Chem. Soc.*, 1952, **6**, 157; (c) J. H. Atherton, Mechanism in two-phase reaction systems: coupled mass transfer and chemical reaction, in R. G. Compton,

G. Hancock (eds.), *Research in Chemical Kinetics*, volume 2, Elsevier, Amsterdam, 1994, p.193.

S39. (a) J. D. Wadhawan, R. G. Evans, C. E. Banks, S. J. Wilkins, R. R. France, N. J. Oldham, A. J. Fairbanks, B. Wood, D. J. Walton, U. Schröder, R. G. Compton, Voltammetry of electroactive oil droplets: electrochemically induced ion insertion, expulsion and reaction processes at microdroplets of *N*,*N*,*N'*,*N'*-tetraalkyl-*para*-phenylenediamines (TRPD, R = *n*-butyl, *n*-hexyl, *n*-heptyl and *n*-nonyl), *J. Phys. Chem. B*, 2002, **106**, 9619; (b) J. D. Wadhawan, R. G. Evans, R. G. Compton, Voltammetric characteristics of graphite electrodes modified with microdroplets of *n*-butylferrocene, *J. Electroanal. Chem.*, 2002, **533**, 71; (c) J. D. Wadhawan, A. J. Wain, A. N. Kirkham, D. J. Walton, B. Wood, R. R. France, S. D. Bull, R. G. Compton, Electrocatalytic reactions mediated by *N*,*N*,*N'*,*N'*-tetraalkyl-1,4-phenylenediamine redox liquid microdroplet-modified electrodes: chemical and photochemical reactions in, and at the surface of, femtolitre droplets, *J. Am. Chem. Soc.*, 2003, **125**, 11418.

S40. (a) M. G. Segal, R. M. Sellers, Reactions of solid iron(III) oxides with aqueous reducing agents, *J. Chem. Soc.*, *Chem. Commun.*, 1980, 991; (b) M. G. Segal, R. M. Sellers, Kinetics of metal oxide dissolution: reductive dissolution of nickel ferrite by tris(picolinato)vanadium(II), *J. Chem. Soc., Faraday Trans. I*, 1982, **78**, 1149; (c) A. Mills, H. L. Davies, M. S. Garley, Kineticsnfor the surface-controlled dissolution of a powder dispersion with a log-Normal distribution in particle size, *J. Chem. Soc.*, *Faraday Trans.*, 1990, **86**, 2163; (d) A. Mills, D. Worsley, Kinetics of redox dissolution of soft-centre particles, *J. Chem. Soc.*, *Faraday Trans.*, 1990, **86**, 3405; (e) A. Mills, P. Sawunyama, Oxidative dissolution of ruthenium dioxide hydrate by periodate ions, *J. Chem. Soc.*, *Faraday Trans.*, 1992, **88**, 2487; (f) C. L. Forryan, O. V. Klymenko, C. M. Brennan, R. G. Compton, Reactions at the solid-liquid interface: surface-controlled dissolution of solid particles: the dissolution of potassium bicarbonate in dimethylformamide, *J. Phys. Chem. B*, 2005, **109**, 2862; (g) C. L. Forryan, O. V. Klymenko, C. M. Brennan, R. G. Compton, Heterogeneous kinetics of the dissolution of an inorganic salt, potassium carbonate, in an organic solvent, dimethylformamide, *J. Phys. Chem. B*, 2005, **109**, 8263; (h) C. L. Forryan, O. V. Klymenko, S. J. Wilkins, C. M. Brennan, R. G. Compton, Experimental and theoretical study of the surface-controlled dissolution of cylindrical particles: application to solubilisation of potassium hydrogen carbonate in hot dimethylformamide, *J. Phys. Chem. B*, 2005, **109**, 20786; (i) C. L. Forryan, R. G. Compton, O. V. Klymenko, C. M. Brennan, C. L. Taylor, M. Lennon, Comparative solubilisation of potassium carbonate, sodium bicarbonate and sodium carbonate in hot dimethylformamide: application of cylindrical particle surface-controlled dissolution theory, *Phys. Chem. Chem. Phys.*, 2006, **8**, 633.